

Visualizing Internal Wave Generation by Finite Cylinder Oscillations using Stereo Particle Image Velocimetry

by

Spencer Wilson

Submitted to the Department of Mechanical Engineering
in partial fulfillment of the requirements for the degree of
Bachelor of Science in Mechanical Engineering

at the

MASSACHUSETTS INSTITUTE OF TECHNOLOGY

June 2015

© Massachusetts Institute of Technology 2015. All rights reserved.

Author
Department of Mechanical Engineering
May 18, 2015

Certified by
Thomas Peacock
Associate Professor
Thesis Supervisor

Accepted by
Gang Chen
Chairman, Department Committee on Undergraduate Theses

Visualizing Internal Wave Generation by Finite Cylinder Oscillations using Stereo Particle Image Velocimetry

by

Spencer Wilson

Submitted to the Department of Mechanical Engineering
on May 18, 2015, in partial fulfillment of the
requirements for the degree of
Bachelor of Science in Mechanical Engineering

Abstract

This thesis investigates internal wave generation in a stratified fluid by means of an oscillating cylinder. We observe the consequences of boundary effects by the production of an out-of-plane velocity field as the cylinder span is decreased. Four cylinders are used. Stereoscopic PIV is utilized for flow visualization and velocity field quantification of the three-dimensional internal wave field evolution. This data is analyzed to determine a relationship between the generation source span as a function of out of plane velocity components in the resultant wave field. As the span of the cylinder is systematically decreased, we observe the evolution of the wave field towards three-dimensionality. To better understand the nature of these boundary effects, a horizontal cylinder is imaged at four location along its length. A tilted cylinder is imaged at its end for two forcing frequencies. These experiments allow a qualitative grounding in the production of wave cones from finite cylindrical generation sources.

Thesis Supervisor: Thomas Peacock
Title: Associate Professor

Acknowledgments

I would like to thank Sasan Ghaemsaedi for his willingness to take on a protege late in the game, and coach that student to victory. His help and patience has been invaluable in this process as a wonderful mentor. I would like to thank Professor Tom Peacock for advising me, and spreading his enthusiasm of internal waves. I would like to thank the ENDlab crew for making me feel at home—Margeaux, Matthieu, Severine, and Hussein. Thank you all. I enjoyed my time working alongside you all.

Contents

1	Introduction	6
1.1	Stratified Fluids	6
1.2	Internal Waves	7
1.3	Wave Propagation	8
1.3.1	Buoyancy Frequency	8
1.3.2	Equations of Motion	9
1.3.3	Dispersion Relation	13
1.3.4	Wave Cones	15
2	Experimental Setup	17
3	Boundary Effects	23
3.1	Overview & Description	23
3.2	Results: $\theta = 30^\circ$	25
3.3	Results: $\theta = 45^\circ$	27
3.4	Discussion	28
4	Wave Cone Production by Finite Cylinders	30
4.1	Overview & Description	30
4.2	Results: Horizontal Cylinders	35
4.3	Results: Tilted Cylinders	36
4.4	Discussion	37
5	Conclusion	40

List of Figures

1-1	Measuring internal waves in the field	7
1-2	Illustration of a fluid parcel	8
1-3	St. Andrew's Cross	15
1-4	Wave cone emanation	16
2-1	Stratification Profiles	18
2-2	Wave tank front view	19
2-3	Microspheres	20
2-4	Wave tank top view with cameras	21
3-1	End Effects Setup in the Wave Tank	24
3-2	Runs 1-4, $\theta = 30^\circ$	26
3-3	Runs 1-4, $\theta = 45^\circ$	27
4-1	Cylinder cross section setup	32
4-2	Oblique setup	33
4-3	Tilted cylinder setup	34
4-4	Horizontal cross sections	35
4-5	Oblique cross section	35
4-6	Tilted cylinder end cross section	36
4-7	Horizontal cylinder simulation	38

Chapter 1

Introduction

When we think of waves, we might imagine throwing a stone into a pond, and watching ripples emanate from the center of the strike point. A wave is an oscillation that transfers energy through a medium over time and space. The pond image deals with surface waves, an interaction of forces along the interface of air and water. Internal waves arise within the ocean by geophysical occurrences due to the stratified nature of the fluid.

1.1 Stratified Fluids

The pebble's striking the water produces a wave due to the density difference at the water-air interface. The pebble's energy begins a tug-of-war between buoyancy and gravity as water is pushed up into the air and travels back down again like a mass on a spring. This density difference is a discontinuous stratification, with two characteristic densities, or strata. The ocean is modeled well by a continuously stratified fluid with two characteristic density gradients[3]. At each depth in the ocean, the density changes due to salinity and temperature. In the laboratory, we emulate the ocean's stratification by filling a tank with varying amounts of saltwater at fixed rates. Just as the water oscillates in air with the pebble example, fluid parcels within the stratified fluid are able to oscillate due to the density gradient. The difference between these internal waves and surface waves is the continuity of

the density distribution. This difference gives rise to startling physical properties of internal waves.

1.2 Internal Waves

Internal waves arise due to oscillations in stratified fluids, in the oceans as well as in collapsing stars[4]. Internal waves occur in the ocean due to energy transfer from the movement of water due to tidal energy over topography[7], as well as from above due to storms. Internal waves are studied and emulated experimentally to determine how energy is transferred in our oceans. This research works to explain phenomena including erosion and mixing. Understanding internal wave phenomena is just one aspect of understanding ocean mixing. Mixing in the oceans is important; it is the cause of undersea density distribution and energy transfer, which effects our planet's climate patterns. Researching internal waves relies on the pillars of any research science: theory, computation, and experiment. This study revolves predominantly around experimentation, where we attempt to reproduce ocean-like conditions in order to study a specific internal wave phenomenon. Data collected in the lab is used to help interpret data collected in the field, as shown in figure 1-1, and vice versa.

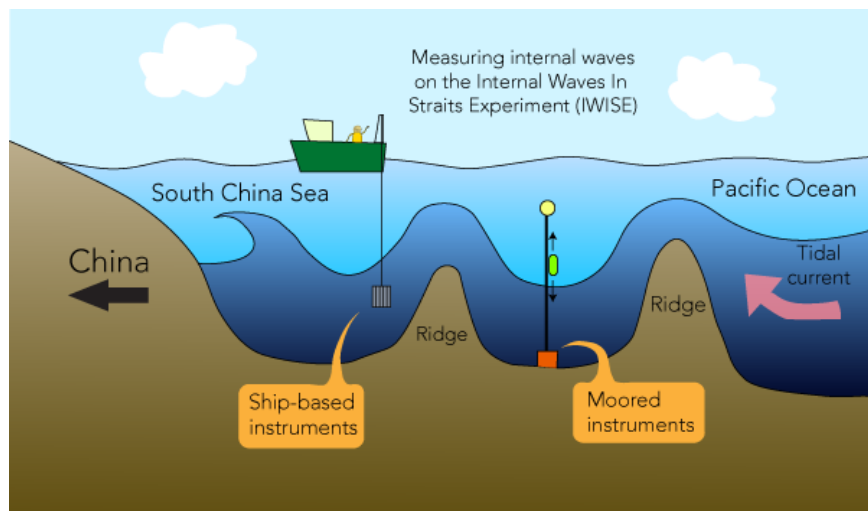


Figure 1-1: A sketch depicting the measurement of internal wave dynamics in the South China Sea. Source: <http://www.michw.com/>

1.3 Wave Propagation

For more insight into internal waves, lays an illustrative foundation of how internal waves propagate. We begin with an explanation of the buoyancy frequency, a value inherent to the stratified fluid which determines the frequency and geometry of the wave field.

1.3.1 Buoyancy Frequency

To find a function relating density to the z direction, we turn to a fluid parcel in a density-stratified medium.

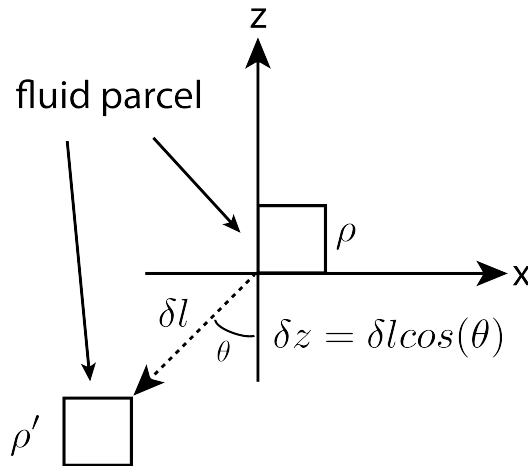


Figure 1-2: Illustration of a fluid parcel displaced in a stratified fluid. The parcel moves to a different region of density ρ' from ρ . This perturbation becomes an oscillation due to buoyancy.

We start with the definition of buoyancy force, arising from fluid density and displace volume V :

$$F_{buoyancy} = \rho(z)Vg.$$

We perturb a particle in the stratified medium, our "ocean", by an infinitesimal amount δz , as shown in figure 1-2. The force that arises is a result of the parcel being in a region of the fluid slightly below its original position where the density is higher. This density gradient is inherent to a gravitationally stable stratification.

$$\rho_o V \frac{\partial^2 \delta z}{\partial t^2} = \rho' V g - \rho V g$$

We cancel terms and rewrite the density as a small change

$$\rho_o \frac{\partial^2 \delta z}{\partial t^2} = -(\delta \rho) g.$$

We have a relationship for the density distribution

$$\delta \rho = -\left(\frac{d\bar{\rho}}{dz}\right) \partial z.$$

Plugging this information in, we have a second-order linear differential equation that represents a harmonic oscillator:

$$\frac{\partial^2 \delta z}{\partial t^2} = -\frac{g}{p_o} \left(\frac{d\bar{\rho}}{dz}\right) \partial z.$$

The natural frequency of oscillation experienced by the fluid parcel is called the buoyancy frequency, N . Buoyancy frequencies are unique to density stratifications and are expressed as:

$$N(z) = \sqrt{-\frac{g}{p_o} \frac{d\bar{\rho}(z)}{dz}}. \quad (1.1)$$

1.3.2 Equations of Motion

Next, the equations of motion for internal waves are derived beginning with a general Navier-Stokes equation in three dimensions x , y , and z . Our specific problem at hand is the oscillation of a cylinder in a density-stratified fluid, where the direction of oscillation is in the direction of the density gradient, namely the z direction. We assume no background flow, only flow from the perturbation introduced by the cylinder oscillation. We assume our fluid is incompressible, and we neglect nonlinear effects. We also assume the fluid is inviscid, citing water as our model fluid. With these considerations, we seek a linear partial differential equation governing our flow field. We assert that the fluid has a linear, hydrostatic pressure profile in the z direction

given by

$$p(\bar{z}) = \int_0^z -\rho g dz.$$

The pressure in the fluid is given by

$$p = p(\bar{z}) + p',$$

where p' is a pressure perturbation. Similarly, the density of the fluid is given by

$$\rho(z) = \rho(\bar{z}) + \rho'(x, y, z, t),$$

where $\rho'(x, y, z, t)$ is a density perturbation.

The velocity components are u, v, w in the x, y, z directions, respectively. The momentum equations in three dimensions can be written in vector form as

$$\frac{\partial \underline{u}}{\partial t} + (\underline{u} \dot{\nabla}) \underline{u} = -\nabla h$$

where u is a general velocity parameter in three dimensions and h is defined as the hydraulic head in the system. We begin with differential equation for the three coordinates of a point in the fluid field:

$$\begin{aligned} \frac{\partial u}{\partial t} + u \frac{\partial u}{\partial x} + v \frac{\partial u}{\partial y} + w \frac{\partial u}{\partial z} &= -\frac{1}{\rho} \frac{\partial p}{\partial x} \\ \frac{\partial v}{\partial t} + u \frac{\partial v}{\partial x} + v \frac{\partial v}{\partial y} + w \frac{\partial v}{\partial z} &= -\frac{1}{\rho} \frac{\partial p}{\partial y} \\ \frac{\partial w}{\partial t} + u \frac{\partial w}{\partial x} + v \frac{\partial w}{\partial y} + w \frac{\partial w}{\partial z} &= -\frac{1}{(\bar{\rho} + \rho')} \left(\frac{d(\bar{p} + p')}{dz} - \rho g \right). \end{aligned}$$

Assuming no background flow and neglecting viscous effects, we replace u, v , and w with u', v' and w' . After substituting and canceling nonlinear terms, we are left with

terms on the order of the perturbation for our three momentum equations

$$\frac{\partial u'}{\partial t} = -\frac{1}{\bar{\rho}} \frac{\partial p'}{\partial x}, \quad (1.2)$$

$$\frac{\partial v'}{\partial t} = -\frac{1}{\bar{\rho}'} \frac{\partial p}{\partial y}. \quad (1.3)$$

$$(1.4)$$

In the z direction, we have:

$$\frac{\partial w'}{\partial t} = -\frac{1}{(\bar{\rho} + \rho')} \left\{ \frac{d(\bar{p} + p')}{dz} - \rho g \right\}.$$

Since p' is much smaller relative to \bar{p} , we are able to neglect it. We also have a relationship between the pressure gradient and the density

$$\frac{dp}{dz} = -\rho g.$$

Combining and substituting, we have a relationship for momentum in the z direction

$$\frac{\partial w'}{\partial t} = -\frac{1}{\bar{\rho}} \frac{\partial p'}{\partial z} - \frac{\rho'}{\bar{\rho}} g.$$

To make the physics simpler, we now invoke the Boussinesq approximation, which states that the density of the fluid field as a function of z is approximately that of the bulk density of the fluid. This means that we are neglecting the small addition of density due to saltwater, but not neglecting the density imposed by the stratification of the fluid. Thus,

$$\bar{\rho}(z) = \rho_o + \tilde{\rho}(z)$$

becomes

$$\bar{\rho}(z) \approx \rho_o.$$

since

$$\bar{\rho}(z) \ll \rho_o.$$

The w momentum equation is now

$$\frac{\partial w'}{\partial t} = -\frac{1}{\rho_o} \frac{\partial p'}{\partial z} - \frac{\rho'}{\rho_o} g. \quad (1.5)$$

Thus, we have our first three momentum equations.

From the buoyancy frequency, we have a relationship

$$\frac{\partial \rho_o}{\partial z} = -N^2 \frac{\rho_o}{g}.$$

This can be substituted into equation (1.5) which becomes

$$\frac{\partial \rho'}{\partial t} + w'(-N^2 \frac{\rho_o}{g}) = 0. \quad (1.6)$$

Our fourth equation is that of continuity. By taking the total derivative of density, we find

$$\frac{D\bar{\rho}}{Dt} = \frac{\partial \bar{\rho}}{\partial t} + \nabla \cdot (\bar{\rho} \underline{u}) = 0$$

which reduces to

$$\frac{\partial \bar{\rho}}{\partial t} + \rho_o(\nabla \cdot \underline{u}) = 0$$

$\bar{\rho}_o$ doesn't depend on time, and can be removed. This leaves the classic form of the continuity equation.

$$\nabla \cdot \underline{u} = \frac{\partial u'}{\partial x} + \frac{\partial v'}{\partial y} + \frac{\partial w'}{\partial z} = 0 \quad (1.7)$$

Our fifth equation is that of incompressibility.

$$\frac{\partial \rho}{\partial t} + \underline{u}' \cdot \nabla \rho = 0$$

We can expand this equation in order to cancel terms that are zero.

$$\frac{\partial \bar{\rho}}{\partial t} + \frac{\partial \rho'}{\partial t} + u' \frac{\partial \bar{\rho}}{\partial x} + v' \frac{\partial \bar{\rho}}{\partial y} + w' \frac{\partial \bar{\rho}}{\partial z} = 0$$

The incompressibility equation reduces to a simpler form. Our fifth equation is

$$\frac{\partial \rho'}{\partial t} + w' \frac{\partial \bar{\rho}}{\partial z} = 0. \quad (1.8)$$

Now we have a system of five equations and five unknowns. We are able to solve the system for a general parameter ψ , the stream function, by imposing two-dimensionality. The stream function is related to the equation of incompressibility, and is defined by the velocity components where u is $\frac{\partial \Psi}{\partial z}$ and w is $-\frac{\partial \Psi}{\partial x}$.

We now have a single linear partial differential equation, the equation of motion for internal wave propagation

$$\partial_{tt}(\nabla^2 \Psi) + N(z)^2 \partial_{xx} \Psi. \quad (1.9)$$

1.3.3 Dispersion Relation

We now obtain a dispersion relation for the wave beams emanating from the cylindrical generation source. We are interested in discovering the vector directions in which energy and phase travel in an internal wave. We have a known ansatz for equation (1.9): a plane wave solution of the form

$$\psi = \psi_0 e^{i(\underline{k} \cdot \underline{x} - \omega t)}.$$

where \underline{k} is the wavenumber vector. We insert this ansatz into equation (1.9) to find a relationship between the wavenumber, the forcing frequency, and the buoyancy frequency

$$\frac{\omega}{N} = \frac{\pm k}{\sqrt{k^2 + m^2}}.$$

In wavenumber space (k, m) , this relationship becomes

$$\frac{\omega}{N} = \pm \sin(\theta)$$

where theta is the angle of \underline{k} with the vertical. The group velocity is defined as

$$\underline{c}_g = \frac{\partial \omega}{\partial \underline{k}} = \nabla_{\underline{k}} \omega.$$

Taking derivatives with respect to the components of \underline{k} , we find the possible directions for internal waves from sign conventions

$$c_g = \frac{Nm}{(k^2 + m^2)^{\frac{3}{2}}} (\mp m, \pm k).$$

From this analysis, we see that the wavenumber vector is orthogonal to the group velocity vector, where the z components are reversed and the x components are the same, as shown in figure 1-3. This is a curious fact, as in our pebble example the group and phase velocities propagate in the same direction. For an oscillating cylinder, internal waves emanate with a wave packet size on the order of the diameter of the cylinder, and propagate in the directions shown in figure 1-3.

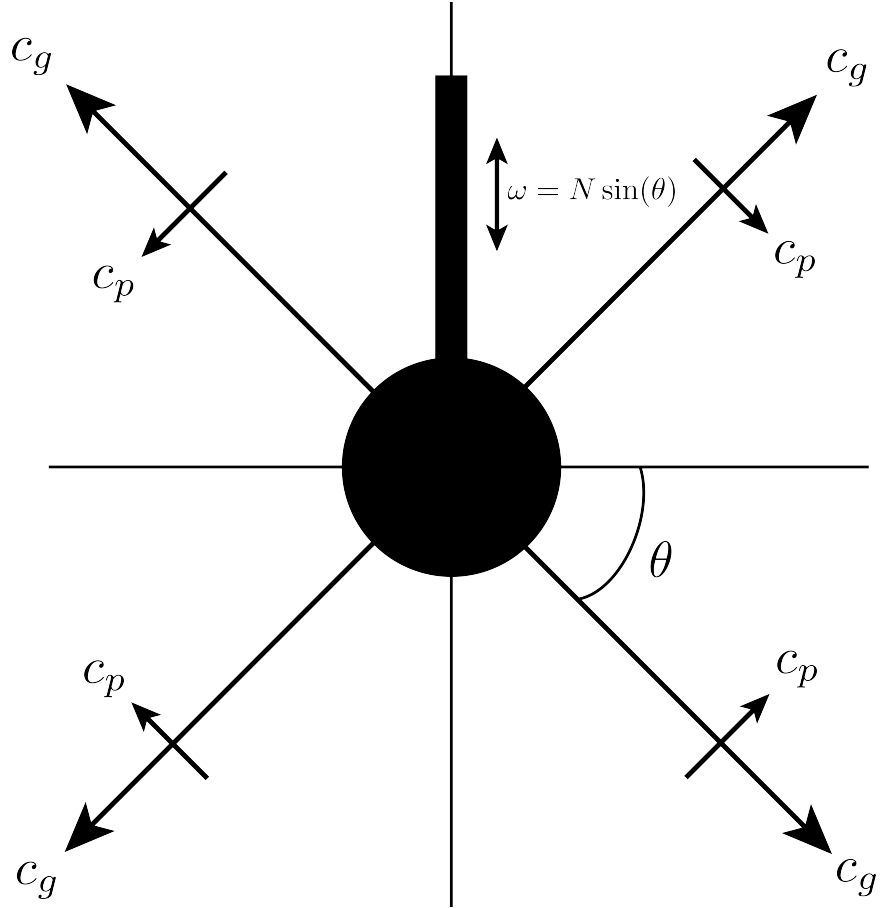


Figure 1-3: Internal waves are produced by oscillating a cylinder in a density stratified medium of buoyancy frequency N . The phase and group velocities emanate perpendicular to one another.

1.3.4 Wave Cones

Because we will be dealing with an open area of research with little prior knowledge, it is productive to introduce the concept of wave cones as we will intend to visualize such topologies. Wave cones are theorized to be the effect of cylinder finiteness during oscillation of a cylindrical body in stratified fluids. This theory is helpful in predicting geophysical phenomena to explain undersea wave generation. The St. Andrew's Cross can be attributed to flows emanating from an infinite cylinder, along its length, where the order of magnitude of the wave beam profile is that of the diameter of the cylindrical source. At the ends of the cylinder, recent work has hypothesized the production of a cone, like the one seen when the body has two radii

of curvature, namely a sphere in our 3-space [2]. In figure figure 1-4, we see the wave beams that emanate from the body of cylinder in red, and the wave cone that is theorized to emanate from the ends in black. The equations governing the shape of these structures are inherently trigonometric, based on the angle of the wave beam θ and the tilt angle of the cylinder ϕ .

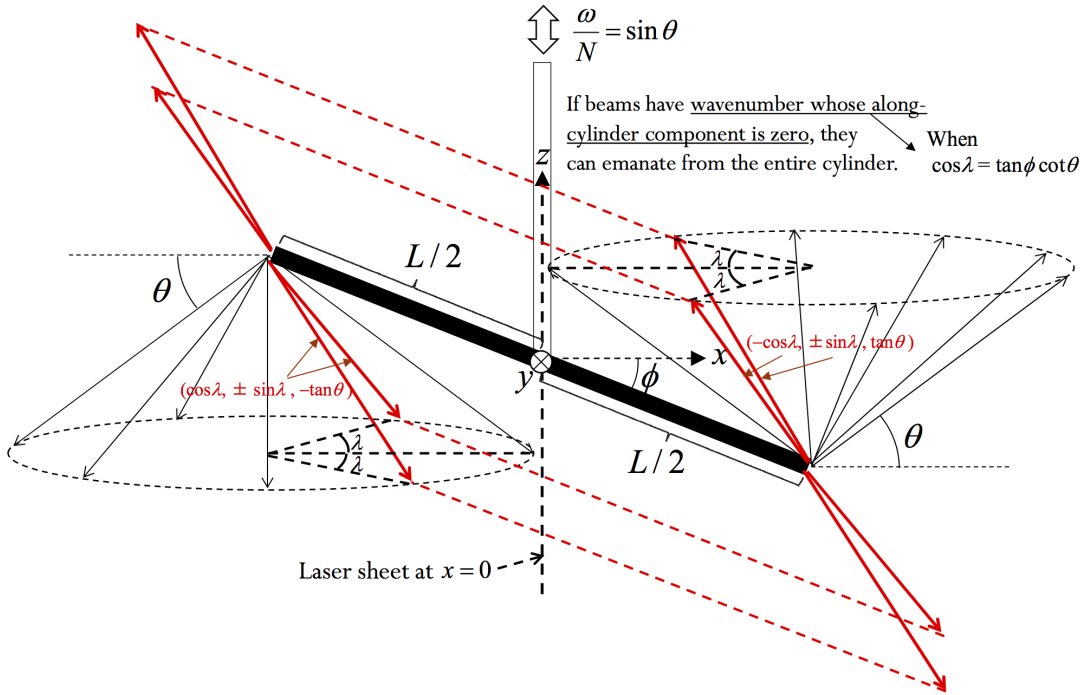


Figure 1-4: Illustration of the theory of wave cone generation. The wave cone is shown in black, and the wave beams propagating from the cylinder's body are shown in red. Figure prepared by Professor Takeshi Kataoka of Kobe University, Japan.

Chapter 2

Experimental Setup

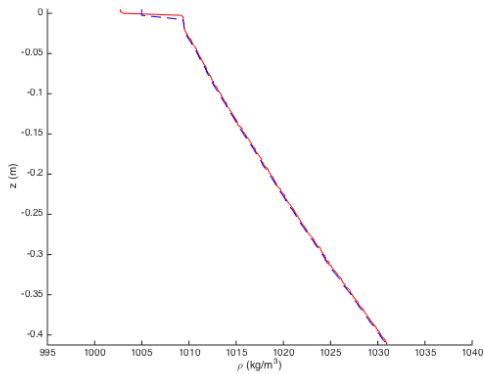
In order to emulate the ocean's stratification a large wave tank is used, as shown in figure 2-2. The size of the tank is an order of magnitude larger than the waves that are produced through oscillations of bodies within the tank, which provides a nice setting to clearly visualize the wave fields.

The tank is 5 m long and 0.5 m wide. The ends of the tank include inset parabolic walls, and the length of the tank includes a wall inset that is adjustable over the tank's width. As a wave field is produced in the tank, waves will reflect off the front wall and the inset wall traveling down the tank's length. When these reflections reach the parabolic insets, they will reflect approximately normal to their point of incidence, traveling behind the inset wall. This way, reflections will not travel back into the field of view and disrupt the visualization. Multiple experiments can be run for a single tank's stratification because inertial effects allow the stratification to settle between experiments. Each experiment in this study employs a linear motor driver with a ball screw for accurate, sub-millimeter movements of a cylinder. Oscillations of the cylinders are on the order of 1mm. The tank is comprised of aluminum T-slot and 1.25cm thick tempered glass for strength and modularity. The internal walls are of acrylic.

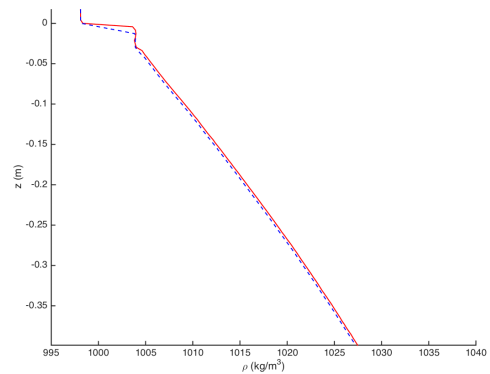
A Parker linear traverse is mounted to the top of the tank. The cylindrical generation sources are attached to the traverse and actuated by sinusoidal harmonic motion. The frame of the traverse is made of aluminum T-slot for rigid attachment to the wave

tank. The cylinders used in these experiments have a diameter of 2.5cm and vary in length from 28cm to 43.7cm.

In order to create a linearly stratified fluid, we utilize the double-bucket technique to gradually increase the salinity as the tank is filled. At each isopycnal, the density must increase by a known amount in order to yield a macroscopic linear stratification across the depth of the tank. To achieve this, one vessel is filled with "heavy" water, water with a higher salt concentration compared to the "light" water bucket. Heavy water is pumped using a peristaltic pump at a known, calibrated flow rate into the light water bucket. Another peristaltic pump moves water at a different known rate into the wave tank. For the stratifications in this study, the heavy water is pumped at $3 \frac{\text{liters}}{\text{sec}}$ and the light water is pumped into the tank at a rate of $6 \frac{\text{liters}}{\text{sec}}$ throughout the filling process. This constant ratio of inputs yields a linear density gradient, and a single buoyancy frequency N for each experiment. The stratification is experimentally measured using a conductivity probe before each experiment to determine the unique N value.



(a) Boundary Effects Stratification



(b) Wave Cone Stratification

Figure 2-1: Plots of fluid density versus depth within the wave tank. (a) Stratification recorded using a conductivity probe and smoothed in software. For the experiments described in chapter 3, the stratification is linear with buoyancy frequency $N=0.74 \frac{1}{\text{sec}}$. (b) The stratification for the experiments described in chapter 4 is also linear, with buoyancy frequency $N=0.78 \frac{1}{\text{s}}$.

For each experiment, a cylinder of varying length and tilt angle ϕ is attached to the

traverse and oscillated at a chosen ω to produce a wave beam traveling at a desired θ with respect to the vertical. This setup is shown as a front view in figure 2-2.

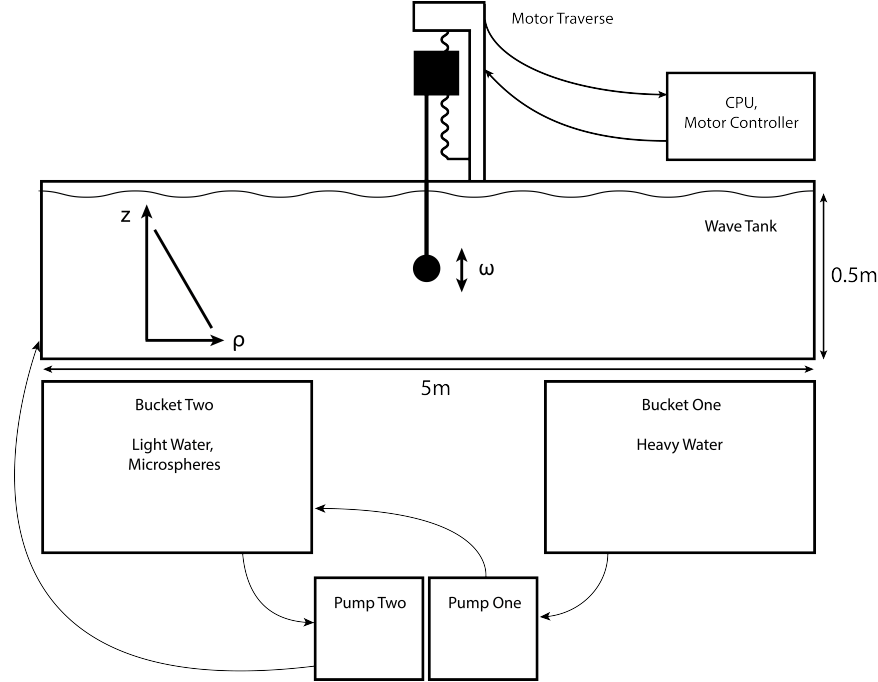


Figure 2-2: Front view of the wave tank setup including a cylinder in the stratified fluid ready for oscillation and imaging.

In order to visualize wave beams produced by cylinder oscillation, special imaging practice must occur. The wave beams, due to their magnitude and the transparency of water, are not visible to the naked eye. Microspheres are added to the light water bucket during filming with digital cameras. The spheres used in this study are manufactured from glass oxide through a series of chemical processes. An example of microspheres is shown in figure 2-3. The particles are on the order of $10\mu m$, and are used to reflect light from a laser sheet positioned under the wave tank. Because the spheres vary in size, their densities vary to allow for settling across the pycnoclines of the stratification. The laser sheet shines from below, through the glass bottom of the wave tank, and into the fluid where that monochromatic light is dispersed by the spheres, appearing as bright spots on a filtered-lens camera.

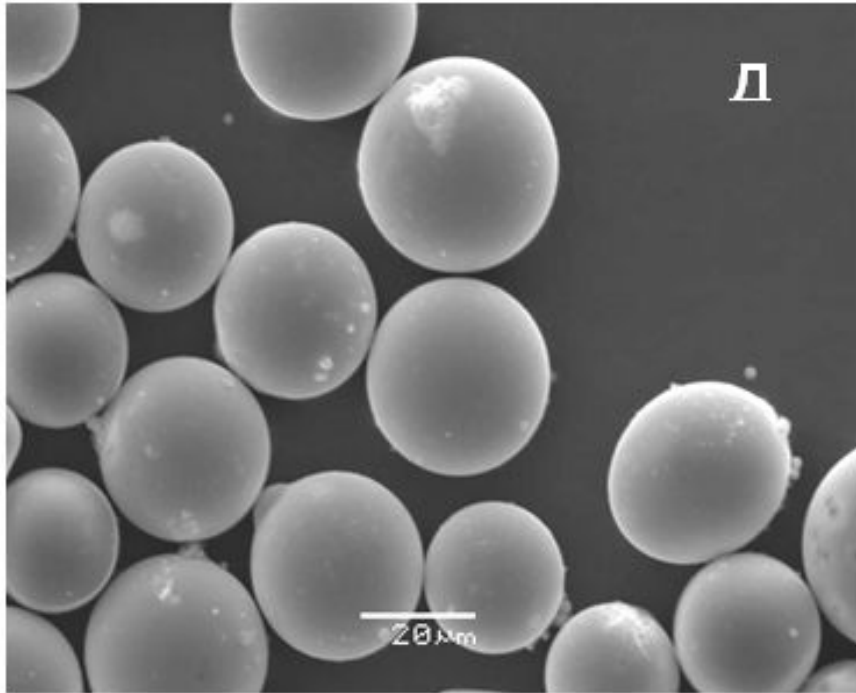


Figure 2-3: An example of microspheres imaged using SEM. Source: <http://ilglass.muctr.ru/>

Two cameras are positioned to create a stereoscopic image of the laser sheet's illumination of the particles within the fluid. When the cylinder oscillates, the particles oscillate within the internal waves that are produced. Images are taken as the LaVision imaging control software triggers the cameras' shutter and the laser at a chosen frequency. A desired number of images are taken, 16 frames per period of oscillation, and saved to the imaging system's hard drive. This constitutes one experiment. The camera setup is shown in figure 2-4 as a top view of the wave tank. This technique has been used extensively as a replacement for Schlieren imaging for visualizing internal wave dynamics[1][6][2]. It has also been used in a variety of fluids research to capture intricate fluid flows around topography[5].

This imagine scheme is stereoscopic particle image velocimetry. Once a number of images are taken over the course of an experiment, they are cross-correlated using the DaVis software package to produce particle velocity vectors. In this way, we are able to visualize how the fluid behaves with energy is inputted into the system un-

der known conditions. For accuracy, each experiment is calibrated with a two-plane calibration plate to offer the software known physical parameters upon which to base the algorithm's velocimetry calculations in three dimensions. Two cameras, like the human eyes, are used to extend our analysis into three dimensions. by tilting one of the cameras and combing the images taken from each, we are able to visualize not only particles moving in the plane of the laser sheet, but out of plane velocities as well. This is important as this study is concerned with the production of out of plane velocities due to cylinder oscillations.

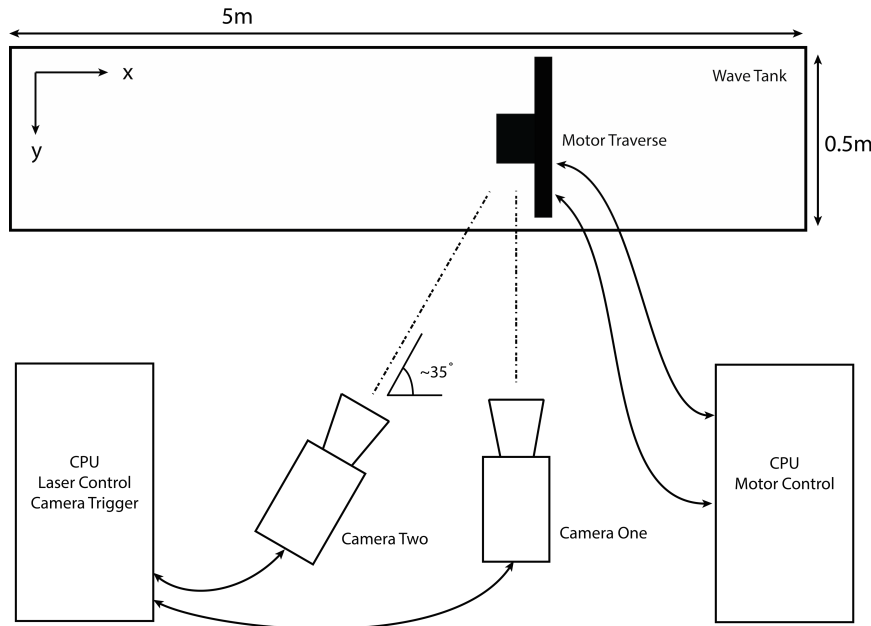


Figure 2-4: Top view of the imaging setup for recording cylinder oscillations for a stereoscopic data collection scheme.

The image data is analyzed using the DaVis software package for stereoscopic output. Once the data is processed through image cross-correlation, it is transferred to MATLAB for Fourier filtering. Each pixel holds a time dependent value for the number of processed images. This discrete time function is Fourier transformed, yielding a function between complex amplitude of the signal and frequency. We know the expected frequency from the experiments, and we sum the amplitude within 20% of this frequency. This amplitude is used to reconstruct a wave field that matches the

experimental data. The filtered data is plotted to visualize the experimental wave fields with less noise.

Chapter 3

Boundary Effects

3.1 Overview & Description

Our first experiment deals with the effects of finiteness with respect to oscillating bodies in stratified fluids. The current theory understanding internal waves and their propagation as discussed in section 1.3 deals with a two-dimensional wave output. This theory does not deal with finite cylinders, or the effects that their ends have on disrupting the classical internal wave field. Typically in analysis, the cylinder is assumed to be in an infinite domain without boundaries to focus on the wave dynamics rather than these end effects. In the geophysical realm however, topographies that give rise to internal wave generation in the oceans are not infinite, and their finiteness is hypothesized to cause energy transfer and mixing. Experiments attempting to reconstruct these geophysical conditions must deal with finite generation sources. Understanding how these end effects manifest in the wave fields is important to understanding how to analyze field data from the oceans and begin to draw conclusions about how oceanic topographies give rise to three-dimensional internal wave generation.

To test the effects of finite cylinders in our experimental setup, four cylinders of varying length used. Experiments 1 through 4 involve oscillating these varying length cylinders at the same frequency. The laser sheet is positioned to coincide with the center of the cylinder for each experiment, and 300 images are taken for each cylinder

at 16 frames per period. The buoyancy frequency for the experiment is $0.74\frac{1}{s}$ and the cylinders were oscillated at an amplitude of 3mm. The runs and the dimensions of the cylinders are shown in figure 3-1. For each of the runs, two frequencies of oscillation were used, $\omega=0.52$ and $\omega=0.37$, which correspond to $\theta \approx 30^\circ$ and 45° respectively.

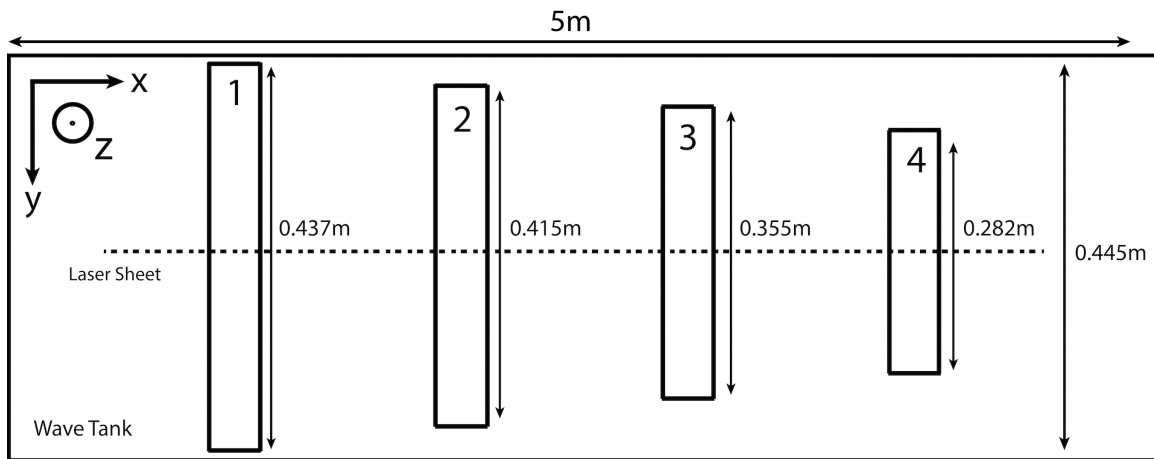


Figure 3-1: End Effects Setup in the Wave Tank

3.2 Results: $\theta = 30^\circ$

The results are organized by run in Figure figure 3-2, where the first row of plots is the longest cylinder with the shortest gaps between the tank's side walls and the ends of the cylinder. For each run, the length of the cylinder is decreased, widening the gap between the side walls and the ends. Data was analyzed for periods 15 through 17 to insure that the measurements reflected a steady state. Plots of the three Fourier filtered velocity components are shown in columns as U, V, and W for the x , y , and z coordinates of the imaging setup as denoted in figure 3-1. The colorbar limits are shown in the Run 4, V component plot, and serve for all other plots.

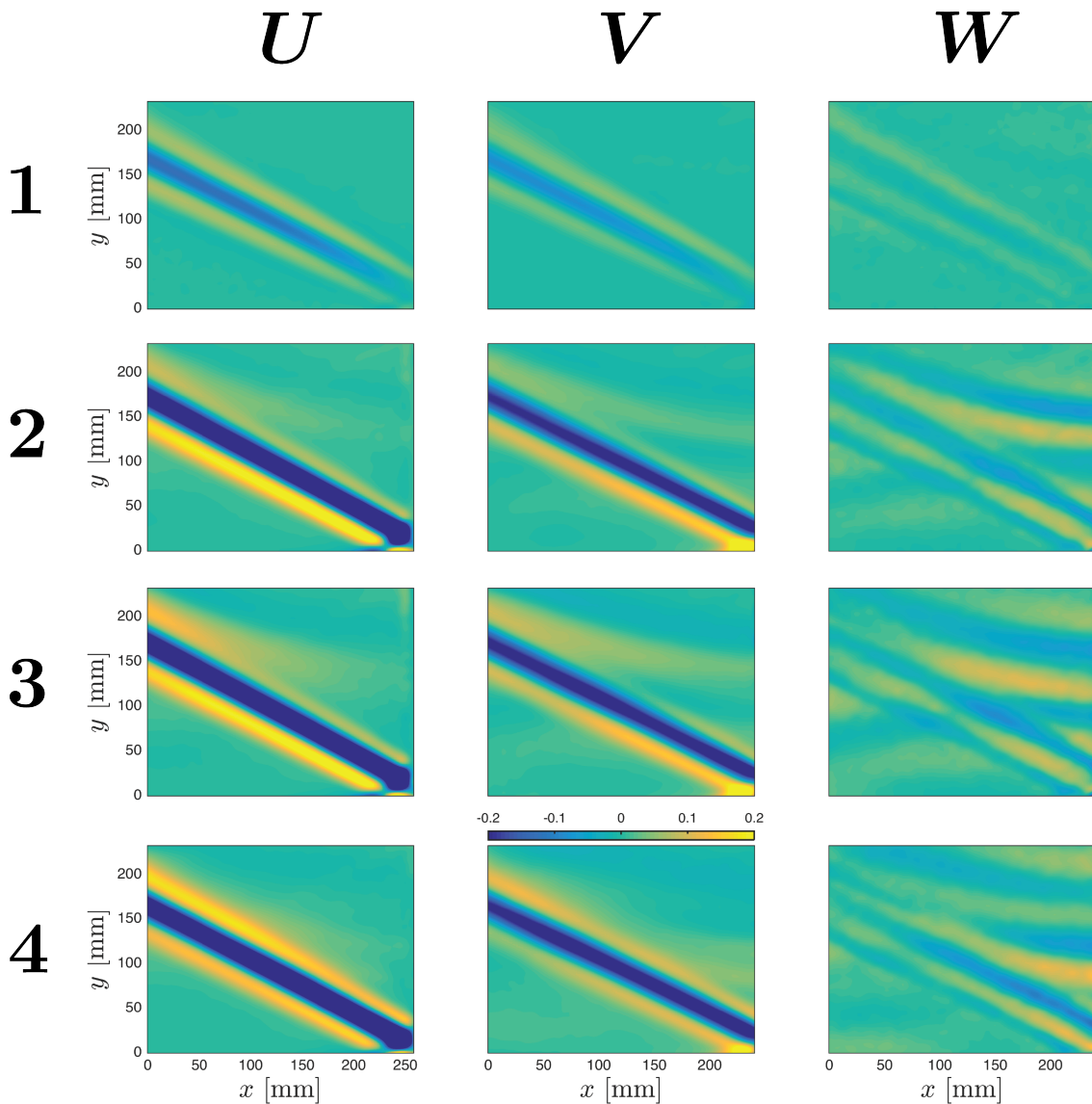


Figure 3-2: Runs 1 through 4 with $\theta = 30^\circ$. The cylinder is centered at the bottom right corner.

3.3 Results: $\theta = 45^\circ$

The results for $\theta = 45^\circ$ are arranged in the same structure as the previous results, where each run is shown on a row and the velocity components of that run are in three columns.

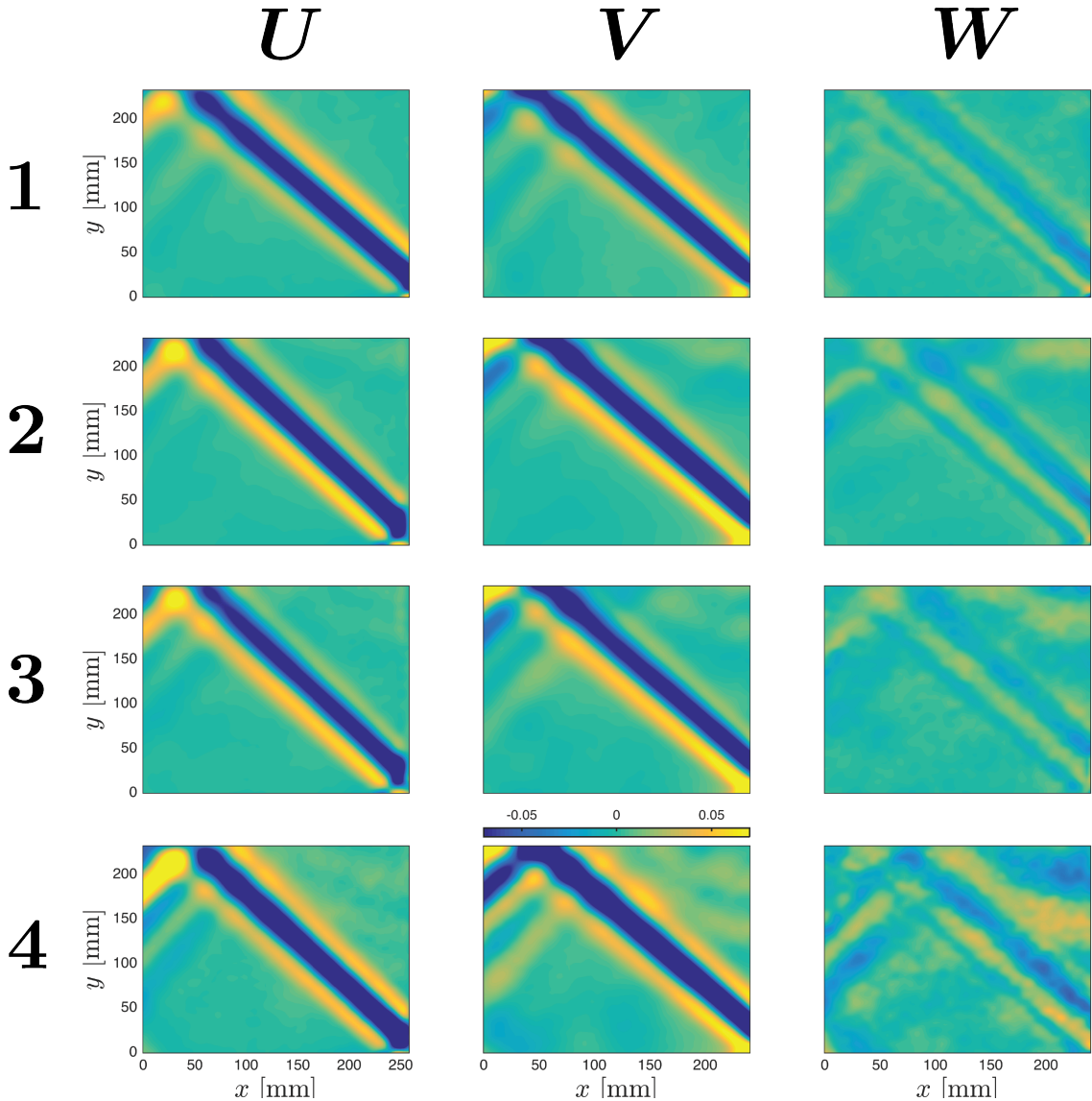


Figure 3-3: Runs 1 through 4 with $\theta = 45^\circ$ for each velocity component. The cylinder is centered at the bottom right corner.

3.4 Discussion

From the plots of the velocities for each dimension, we can see an expected wave beam in the U and V components, emanating from the horizontal cylinders imaged at their center. The amplitude remains constant for each test, and the magnitude of the wave fields are comparable as well. The most interesting aspect of this experiment is the out of plane velocities. Due to the nature of our model, we limit ourselves to two dimensions with our stream function, ψ . These out of plane velocities arise due to the finite nature of the cylinders, and are born from pressure differences as the cylinder oscillates. As the cylinder is shortened in the tank, the characteristics of the distorted wakefield in the z dimension are more pronounced. We can see, following the column in figure 3-2 and figure 3-3, that as the cylinder's length in the tank is reduced, the out of plane velocities take on a structure with higher magnitude. For both set of four runs, a nonlinear structure forms above the cylinder, increasing in magnitude in the top right corner of each W component figure. This is hypothesized as a wave cone, a production linked to end effects.

We offer an explanation for this fact, using scaling arguments between the length scale of the wave field and the viscous effects of the fluid. If we posit that the time varying effects of the fluid dynamics are much larger than the viscous terms in the Navier-Stokes equations, we can derive the scaling argument

$$\frac{\partial u}{\partial t} \gg \nu \frac{\partial^2 u}{\partial z^2}.$$

Our time scale can we attributed to the frequency of our cylinder oscillations, ω , and the characteristic length of the resultant waves is the wavenumber k . Thus the velocity is the division of frequency and wavenumber

$$\left(\frac{\omega}{k}\right)\omega \gg \frac{\nu(\frac{\omega}{k})}{l^2}.$$

Where l is the finite length scale of the z dimension, which must be on the order of

the wavenumber as

$$l \sim \frac{1}{k}.$$

Substituting and simplifying we have a relationship between the wavenumber vector, the frequency, and the kinematic viscosity of the fluid where

$$k \ll \sqrt{\frac{\omega}{\nu}}.$$

In order to neglect end effects due to viscosity, the relationship must hold. In Run 1, we have a length scale on the order of millimeters with respect to the end gap. By our scaling argument, the length scale of the wavenumber vector must be much smaller than approximately 1.4mm based on the dynamic viscosity of water and the forcing frequency. Thus, Run 1 should show minimal out of plane velocities as the length scale of the disturbance in this dimension meets our criterion. This can be seen in the first row of figure 3-2 and figure 3-3. As the gap is increased, we no longer satisfy the scaling argument and, as shown in Runs 2-4. This analysis warrants more complex models of finite topographies, which are a current area of research. The experiments shown here support work towards a physical model of finite topography to better understand realistic undersea geophysical wave dynamics. The next chapter attempts to visualize wave cone production for horizontal cylinders and tilted cylinders.

Chapter 4

Wave Cone Production by Finite Cylinders

4.1 Overview & Description

The purpose of this experiment is to visualize out of plane velocity field production in three spatial dimensions as the laser sheet is moved towards the cylinder's end. We attempt to visualize a wave cone production along a cylinder to further our understanding of its production. The theoretical framework for this idea is current research, and having experimental images to compare theory to is important for the advancement of theory. We expect to see, as the laser sheet is moved towards the end of an oscillating cylinder, a change in its out-of-plane velocity component as a wave cone is gradually intercepted by the visualization plane at different points. Visualizing this wave cone production for horizontal cylinders allows for a better understanding of out-of-plane velocities in geophysical wave generation. These experiments begin with horizontal cylinders and move to tilted cylinders to explore wave cone generation for more advanced topographies.

The design of the experiment is similar to the experiments surrounding the exploration of end effects. Each cylinder was fixed to the linear traverse and oscillated at an amplitude of 3mm for a chosen frequency ω to produce a wave field with a desired θ . For the 28cm horizontal cylinder in this experiment, the laser sheet was moved to

different locations along the cylinder to visualize the wave field at different locations. Each run used a different laser sheet location, and was calibrated separately by placing the calibration plate at a marked location under the tank after all experiments were completed. This setup is shown in figure 4-1. A cylinder was at an oblique angle that corresponds to the movement of the light sheets from the horizontal cross section experiments. The angle of the cylinder was calculated from basic trigonometric relationships between the length of the cylinder and the distance between light sheet cross sections. This setup is shown in figure 4-2. Moving to a tilted regime, a cylinder of pitch angle 28° was chosen for oscillation at two different wave beam angles, $\theta = 30^\circ$ and $\theta = 45^\circ$. This cylinder was imaged at its end as shown in figure 4-3.

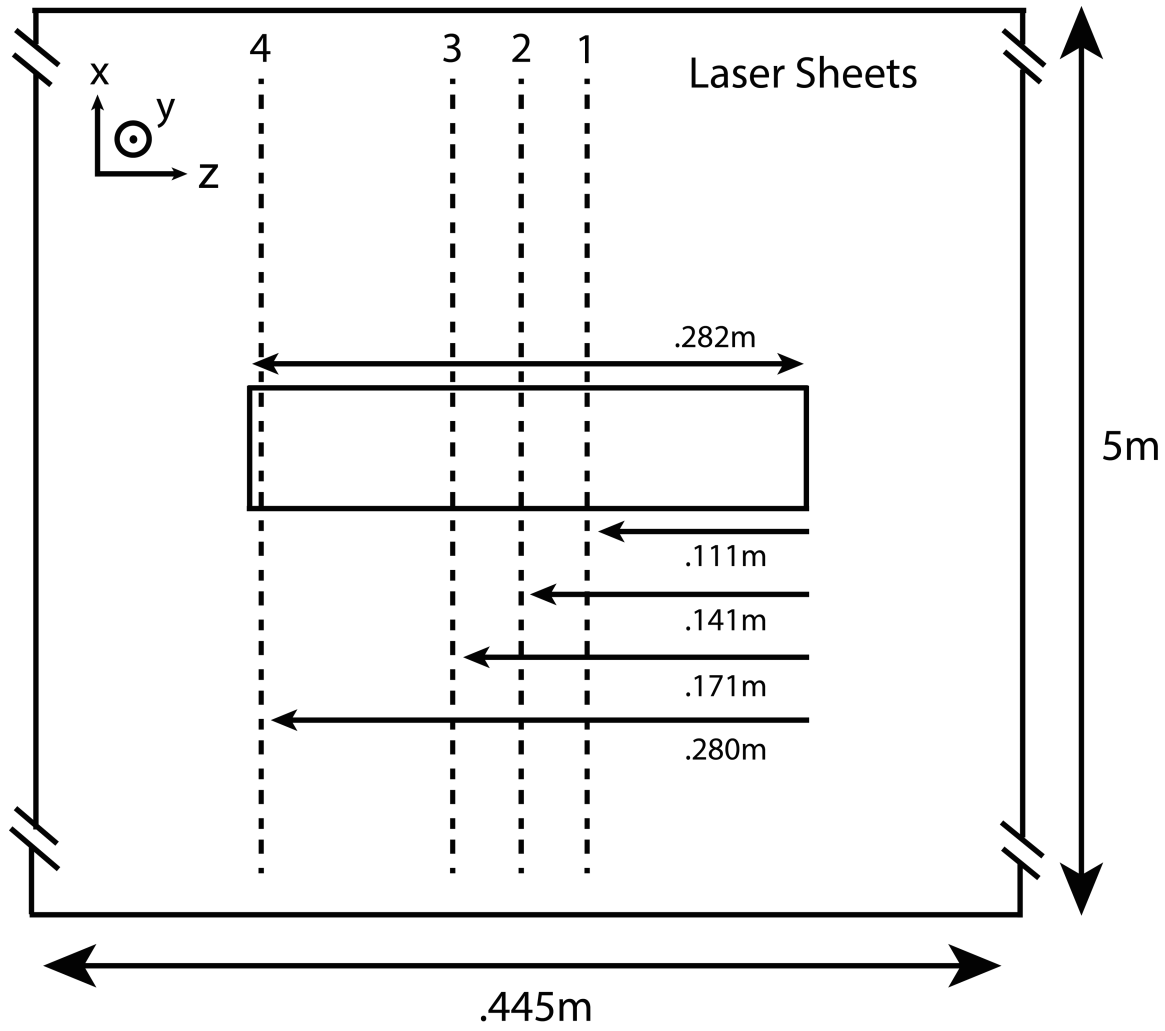


Figure 4-1: Top view of the wave tank with the laser sheet positions shown as dotted lines. Each experiment was run with the laser sheet moved to a new position while the cylinder was left unmoved.

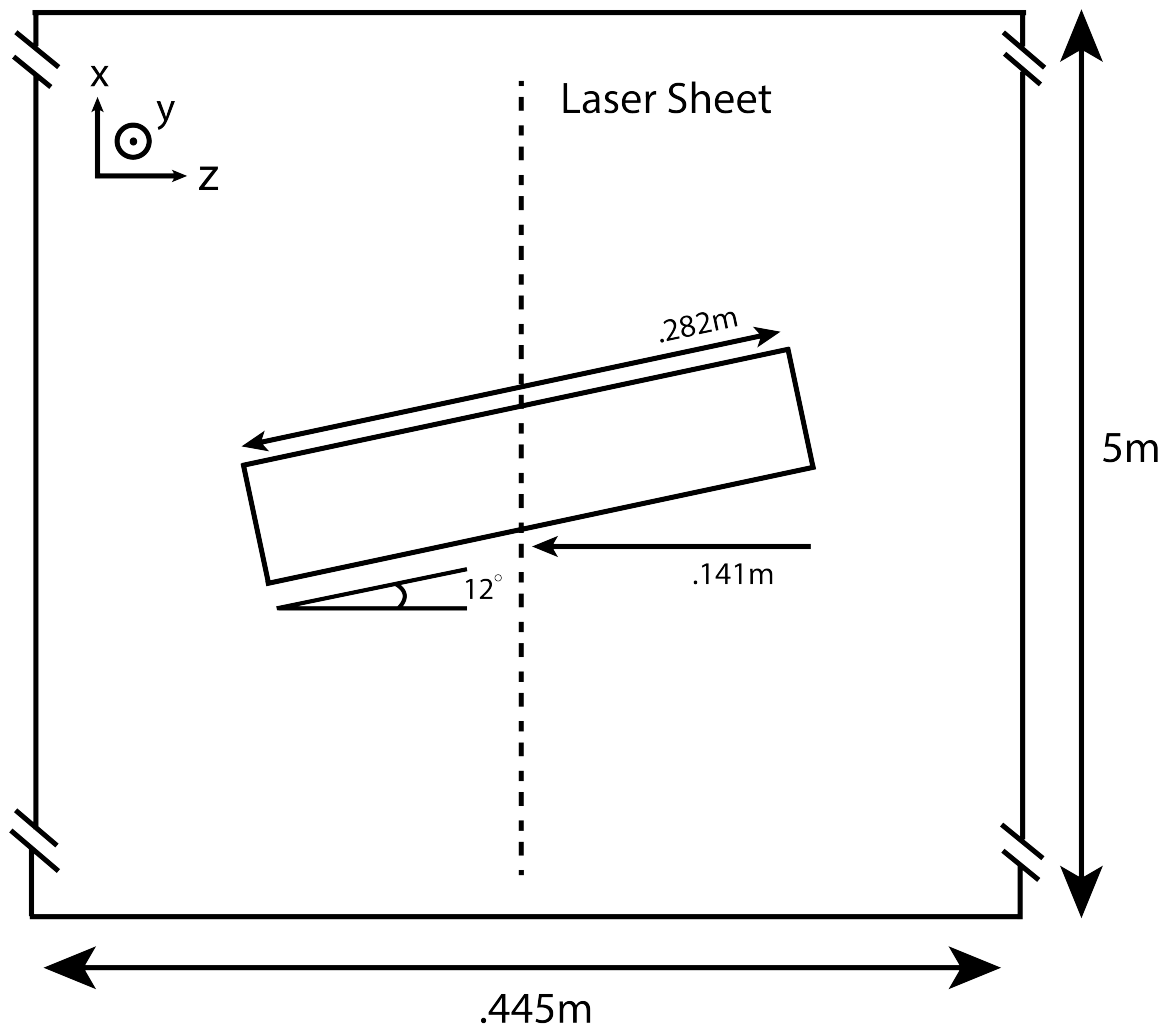


Figure 4-2: To confirm the three dimensions of the laser sheet crosses, the cylinder was turned to cover the full motion of the laser sheet, 12°

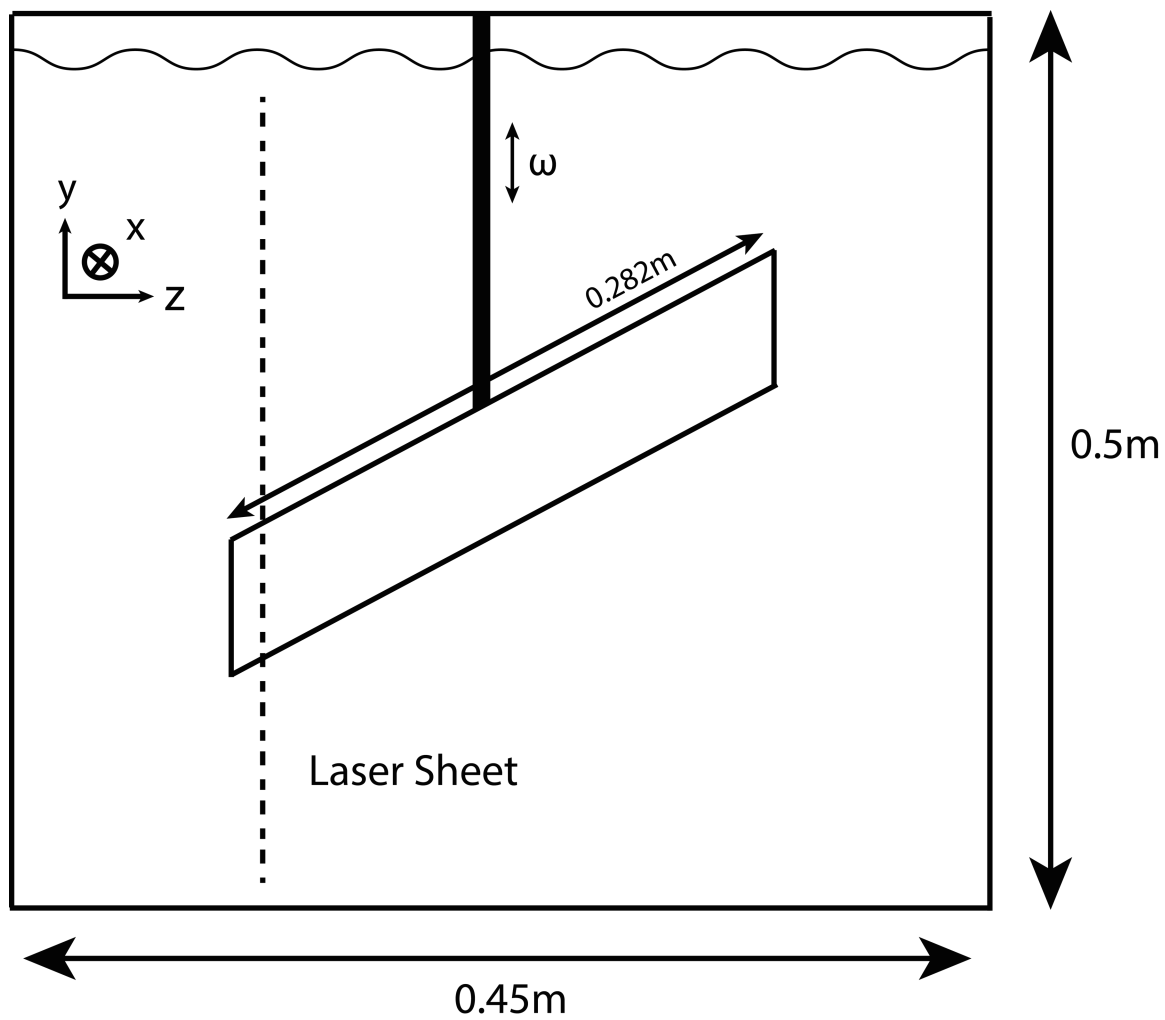


Figure 4-3: Experimental setup of the tilted cylinder tests, visualized at the end of the cylinder for two oscillation frequencies.

4.2 Results: Horizontal Cylinders

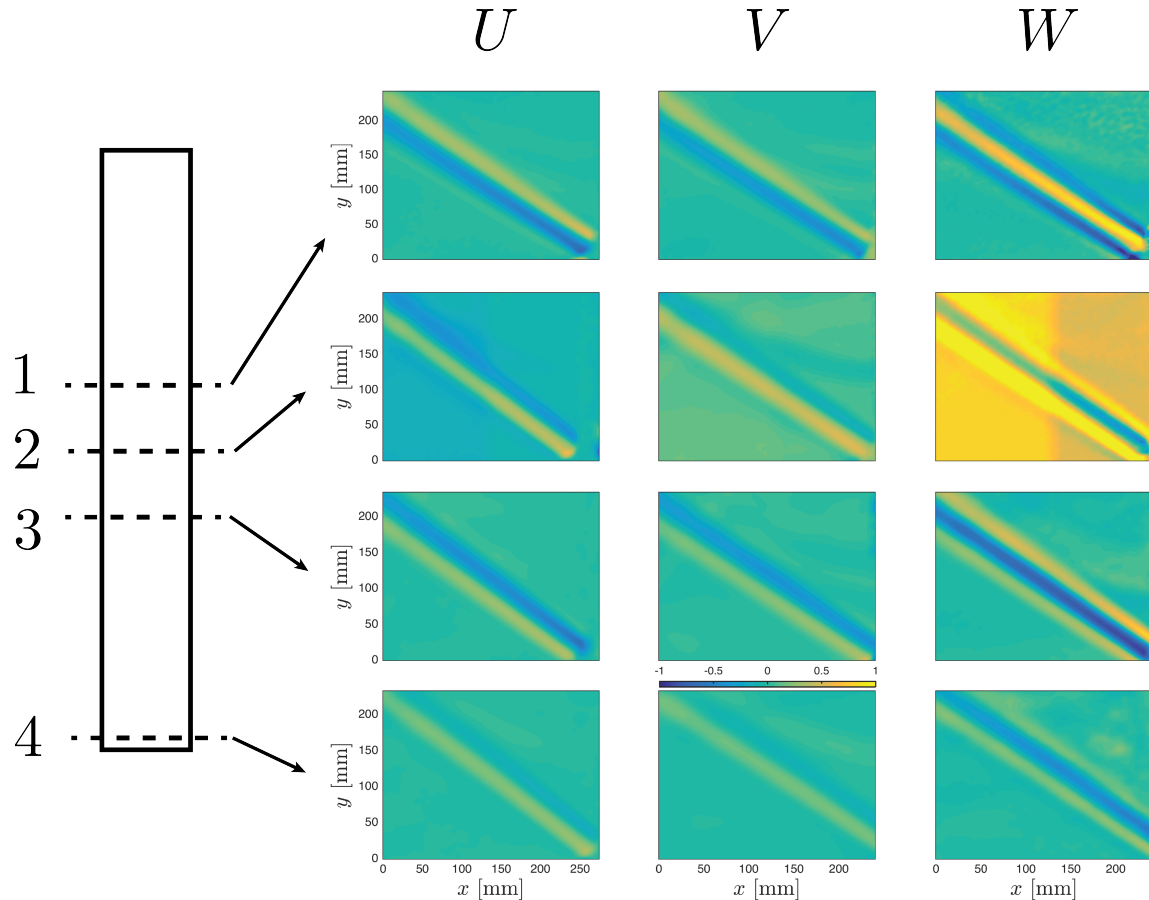


Figure 4-4: Cross section experiments for horizontal cylinder oscillating with $\theta = 37.5^\circ$. Rows shows cross sections 1-4 as denoted in Figure figure 4-1

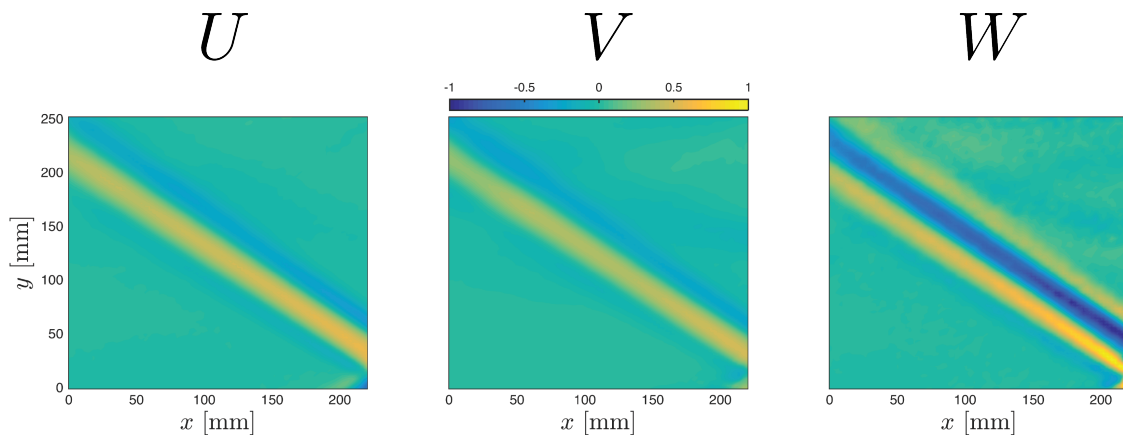


Figure 4-5: Oblique Test, Cross Section along the middle $\theta = 37.5^\circ$

4.3 Results: Tilted Cylinders

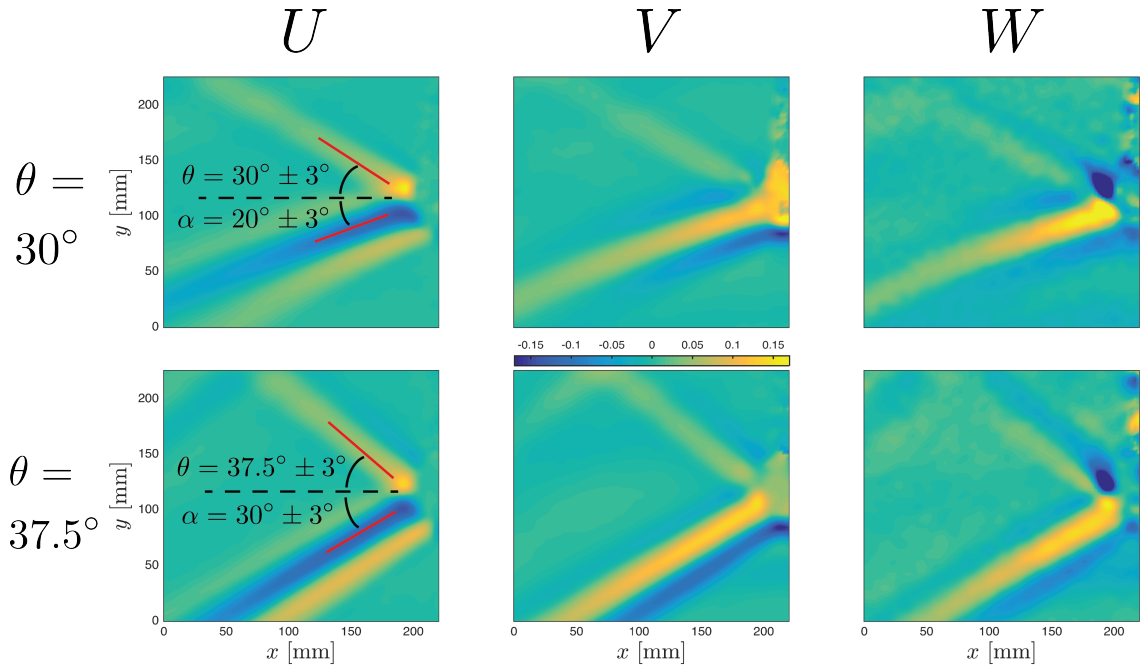


Figure 4-6: Tilted Cylinder, visualized at its end, $\phi = 28^\circ$. Top row is at $\theta = 30^\circ$, bottom row is at $\theta = 37.5^\circ$

4.4 Discussion

From figures figure 4-4, we see clear evidence of wave cone production in the U and V velocity fields as we move towards the end of the cylinder, specifically in the upper right portion of the image. In the third row, a hyperbolic structure is clear in the V component image. This cone is not a reflection, but geometrically shown to be emanating from the end of the cylinder being imaged. This cross section cuts into the cone off-center, thus hyperbolic in nature. The W velocity components, are stronger in magnitude than their in-plane velocities U and V. Additionally, cross section 1's W component is out of phase with respect to cross section 3. We hypothesize an interaction between the out-of-plane velocities along the cylinder from each end. At the center, cross section 2, we see a great increase in magnitude for the out of plane velocities, which is attributed to this interaction. For cross section 4, we notice a noisier W component, which is attributed to heightened end effects. Due to this hypothesis, the oblique experiment shown in figure 4-5 do not correlate with the cross sectional images, expectedly. The oblique experiment is based on a previous theory excluding interactions at the center of a cylinder to produce out of plane velocities, and thus cannot validate these results. In figure 4-5 we see stronger out of plane velocities due to the oblique angle, but do not see out of plane interactions due to the angle of the light's sheet incidence on the cylinder. We hypothesize that the orthogonality of the light sheet in the cross section experiments provides visualization of out of plane interaction.

We are able to simulate the linear solution to our governing equations given the geometries proposed in figure 1-4. A plot of this solution is given in figure 4-7. The top row of plots is taken at the center of a horizontal finite cylinder of length 28cm and diameter 2.5cm, oscillating with a $\theta = 37.5^\circ$. The second row of plots is for 3cm off center along the cylinder, identical to the experiment described in figure 4-1 for Run 1. We see a qualitative similarity between these simulated results and the experimental results, in that the magnitude of the out-of-plane velocity components are as great as the in-plane, as well as the production of a wave cone of lesser magnitude. In the

experiment, we expect noise and nonlinearity to increase the interactions between the out of phase velocity components from either end of the cylinder, whereas in the simulation we see only linear interactions, such as the u velocity component canceling to zero. In our experimental data, we see a faint u component of the wave beam.

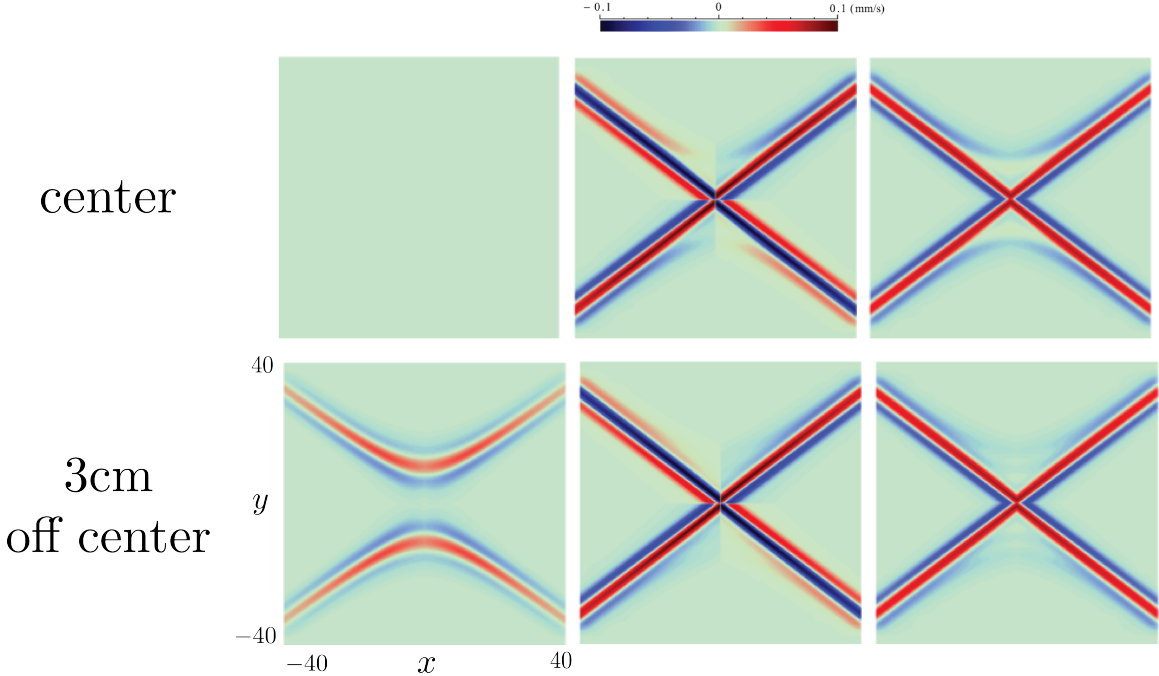


Figure 4-7: Simulation of linear solution for a finite horizontal cylinder, length 28cm and diameter 2.5cm for $\theta = 37.5^\circ$. The top row of plots is at the cylinder's center, the second row is 3cm away from the end. Source: Professor Takeshi Kataoka.

The tilted cylinder experiments show great promise in visualizing the wave cone generation at the cylinder's ends. As shown in figure 4-6, nonlinear structure is seen as the wave beam being emitted along the cylinder mixes with the wave cone being produced at the cylinder's end, producing the hyperbolic wave field as seen near the cylinder in the right-half of the image, midway down the figure. The angles were measured in software, and an error is given to the measurement as a result of error in the aspect ratio of the image and the trigonometric calculation. We see that the linear wave beam propagating along the length of the cylinder is approximately the expected value by the St. Andrew's cross, while the wave cone bends the beam to a lesser value than the oscillation frequency. This lesser angle is an open area of research as to its existence and the relationship governing this beam angle as a function of ϕ

and oscillation frequency. Thus, we have confirmed the existence of the linear wave beam propagating in the form of a St. Andrew's cross as shown in figure 1-3 along the cylinder until its end, where nonlinear effects occur. At the end, we see the production of a wave cone, which is supported by the horizontal experiments as seen in figure 3-2.

Chapter 5

Conclusion

This thesis has dealt with wave field generation within stratified fluid by a cylindrical generation source, particularly the effects of finiteness on wave topologies. We have shown for two oscillating frequencies within the pass band set by the fluid's experimental buoyancy frequency, out of plane velocities diminish as the generation source becomes pseudo-infinite, spanning the width of the wave tank leaving a gap that meets the criterion set by the fluid viscosity. From this experiment, we learn the importance of finiteness in our internal wave model, and seek to understand its effect. This finiteness is important to eliminate idealizations in our geophysical model. Cylindrical generation sources are ideal ridges within the ocean, oscillating with tidal movements. Undersea topographies are highly nonuniform, and finite with respect to edges and other features. Thus, this experiment in the boundary effects proves the importance of researcher nonuniform topographies in the laboratory to gain insight in the geophysical realm. In addition, understanding boundary effects provide case studies for parsing new data. It is known now that finite cylinders produce out of plane velocity components, and future experiments may utilize this result in comprehending wave fields produced by nonuniform topographies.

To further the understanding of boundary effects, we wish to trace their origin along a horizontal cylinder. We see the effects of finiteness when imaging at the center of an oscillating cylinder, and imaging across four planes orthogonal the cylinder provides a better illustration of how these out of plane velocities are produced. We cite the

phase difference between each side the cylinder as an indication of an interaction at the cylinder's center. The out of plane velocities at the center of the source may arise due to interactions from each cylinder's end, producing wave fields of higher magnitude in the W velocity component. The horizontal cylinder is then imaged at its end to confirm the existence of a wave cone in the U and V velocity components as well as the disturbance of the wave field in the W component due to boundary effects investigated in Chapter 3. These experiments support the wave cone hypothesis, as well as introduce the interaction of waves due to cylinder finiteness. We posit, then, of self-interactions in the geophysical realm for nonuniform topographies, where out of plane velocities may interact and grow in magnitude to incite greater energy transfer and mixing.

To further investigate the wave cone theory, we visualize a tiled cylinder at its end for two oscillating frequencies. The images show the nonlinear structure of the hyperbolic wave cone, and its effect on the angle of emanation from the cylinder. We are able to ascertain the effect of oscillation near the resonant frequency, the angle ϕ in the 30° image. From these images, we are able to see the coexistence of linear wave beams emanating from the length of the cylinder, and interacting with the wave cone at the cylinder's end, as our theory predicts. These results are important for understanding undersea topographies with varying elevation, which may lead to interaction between linear wave fields and wave cones at areas with ridges, for example.

The work presented here is meant to be both an encapsulation of experimental and theoretical concepts concerning the production of internal waves in a stratified medium by cylindrical generation sources and a presentation of novel research into the theory of boundary effects on internal wave fields. The purpose of this work is to step closer to understanding energy transfer in the oceans through undersea waves. Through tidal movements or other energy inputs, the energy is a large and complex system of energy transport processes. We strive to reproduce pieces of this system in the laboratory to discover how our environment physically changes. This work moves us a step closer to moving our model away from idealizations by visualizing the consequences of realistic domains. Namely, the acceptance of a finite generation

sources and the consequences of such as seen in the resultant wave fields. This work aims to provide insight for future studies in visualizing more complex geometries and interactions within stratified fluids with respect to experimental design and practice.

Bibliography

- [1] Ch. Brücker. 3-D scanning-particle-image-velocimetry: Technique and application to a spherical cap wake flow. *Appl. Sci. Res.*, 56(2-3):157–179, 1996.
- [2] Sasan John Ghaemsaidi and Thomas Peacock. 3D Stereoscopic PIV visualization of the axisymmetric conical internal wave field generated by an oscillating sphere. *Exp. Fluids*, 54(2), 2013.
- [3] Manikandan Mathur and Thomas Peacock. Internal wave beam propagation in non-uniform stratifications. *J. Fluid Mech.*, 639:133, 2009.
- [4] Josefina Montalban and Evry Schatzman. Mixing by internal waves. III. Li and Be abundance dependence on spectral type, age and rotation. *Astron. Astrophys.*, 959:943–959, 2000.
- [5] J. Sakakibara, M. Nakagawa, and M. Yoshida. Stereo-PIV study of flow around a maneuvering fish. *Exp. Fluids*, 36(2):282–293, 2004.
- [6] B. Wieneke. Stereo-PIV using self-calibration on particle images. *Exp. Fluids*, 39(2):267–280, 2005.
- [7] H. P. Zhang, B. King, and Harry L. Swinney. Experimental study of internal gravity waves generated by supercritical topography. *Phys. Fluids*, 19(9):096602, 2007.